



Springer

Dear Author:

Please find attached the final pdf file of your contribution, which can be viewed using the Acrobat Reader, version 3.0 or higher. We would kindly like to draw your attention to the fact that copyright law is also valid for electronic products. This means especially that:

- You may print the file and distribute it amongst your colleagues in the scientific community for scientific and/or personal use.
- You may make your article published by Springer-Verlag available on your personal home page provided the source of the published article is cited and Springer-Verlag and/or other owner is mentioned as copyright holder. You are requested to create a link to the published article in Springer's internet service. The link must be accompanied by the following text: "The original publication is available at springerlink.com". Please use the appropriate DOI for the article. Articles disseminated via SpringerLink are indexed, abstracted and referenced by many abstracting and information services, bibliographic networks, subscription agencies, library networks and consortia.
- Without having asked Springer-Verlag for a separate permission your institute/your company is not allowed to place this file on its homepage.
- You may not alter the pdf file, as changes to the published contribution are prohibited by copyright law.
- Please address any queries to the production editor of the journal in question, giving your name, the journal title, volume and first page number.

Yours sincerely,

Springer-Verlag

A prototype small CdTe gamma camera for radioguided surgery and other imaging applications

Makoto Tsuchimochi¹, Harumi Sakahara², Kazuhide Hayama¹, Minoru Funaki³, Ryoichi Ohno³, Takashi Shirahata³, Terje Orskaug⁴, Gunnar Maehlum⁴, Koki Yoshioka⁴, Einar Nygard⁴

¹ Department of Oral and Maxillofacial Radiology, The Nippon Dental University School of Dentistry at Niigata, Niigata, Japan

² Department of Radiology, Hamamatsu University School of Medicine, Hamamatsu, Japan

³ Acrorad Co. Ltd., Tokyo, Japan

⁴ Integrated Detector & Electronics A.S (IDE AS), Hovik, Norway

Received: 20 February 2003 / Accepted: 7 July 2003 / Published online: 23 September 2003

© Springer-Verlag 2003

Abstract. Gamma probes have been used for sentinel lymph node biopsy in melanoma and breast cancer. However, these probes can provide only radioactivity counts and variable pitch audio output based on the intensity of the detected radioactivity. We have developed a small semiconductor gamma camera (SSGC) that allows visualisation of the size, shape and location of the target tissues. This study is designed to characterise the performance of the SSGC for radioguided surgery of metastatic lesions and for other imaging applications amenable to the smaller format of this prototype imaging system. The detector head had 32 cadmium telluride semiconductor arrays with a total of 1,024 pixels, and with application-specific integrated circuits (ASICs) and a tungsten collimator. The entire assembly was encased in a lead housing measuring 152 mm×166 mm×65 mm. The effective visual field was 44.8 mm×44.8 mm. The energy resolution and imaging aspects were tested. Two spherical 5-mm- and 15-mm-diameter technetium-99m radioactive sources that had activities of 0.15 MBq and 100 MBq, respectively, were used to simulate a sentinel lymph node and an injection site. The relative detectability of these foci by the new detector and a conventional scintillation camera was studied. The prototype was also examined in a variety of clinical applications. Energy resolution [full-width at half-maximum (FWHM)] for a single element at the centre of the field of view was 4.2% at 140 keV (^{99m}Tc), and the mean energy resolution of the CdTe detector arrays was approximately 7.8%. The spatial resolution, represented by FWHM, had a mean value of 1.56±0.05 mm. Simulated node foci could be visualised clearly by the SSGC using a 15-s acquisi-

tion time. In preliminary clinical tests, the SSGC successfully imaged diseases in a variety of tissues, including salivary and thyroid glands, temporomandibular joints and sentinel lymph nodes. The SSGC has significant potential for diagnosing diseases and facilitating subsequent radioguided surgery.

Keywords: CdTe – Gamma camera – Semiconductor – Sentinel lymph node biopsy – Radioguided surgery

Eur J Nucl Med Mol Imaging (2003) 30:1605–1614
DOI 10.1007/s00259-003-1301-3

Introduction

Radioguided surgery is being used at many cancer institutions and teaching hospitals. This relatively new procedure involves accumulation of a radiopharmaceutical into a target tissue, which allows detection of the lesion or cancer by a radiosensitive probe. Radioimmunoguided procedures have also been used in colorectal applications to enable the surgeon to detect lesions or target tissues more accurately [1]. Sentinel lymph node biopsy is the most established of the radioguided surgical procedures and is becoming the standard of care for patients with melanoma [2, 3]. Many surgeons are also applying this technology to breast cancer surgery [4, 5].

To date, a hand-held gamma probe has been used to identify one or more sentinel lymph nodes. However, a gamma probe can only provide radioactivity counts and variable pitch audio output based on the intensity of the detected radioactivity. We suggest that direct visualisation of the spatial distribution of the increased radioactivity would allow more accurate delineation of the surgical field, thereby facilitating surgery.

A gamma camera that is miniaturised or hand-held offers easier application in the restricted space of an oper-

Makoto Tsuchimochi (✉)

Department of Oral and Maxillofacial Radiology,
The Nippon Dental University School of Dentistry at Niigata,
1-8 Hamaura-cho, 951-8580 Niigata, Japan
e-mail: tsuchimochi@ngt.ndu.ac.jp
Tel.: +81-25-2671500 ext 224, Fax: +81-25-2330307

ating field. A solid-state detector is suitable for this purpose. Because a solid-state detector can transduce gamma photons directly into a digital electronic signal, there is no need for the cumbersome two-step process required when employing more conventional gamma cameras. The older technology requires initial conversion of the gamma ray to light in a sodium iodide scintillation crystal followed by changing of the light into an electric charge by passing it through the photomultiplier tube. In general, semiconductor detectors suffer poorer intrinsic detector sensitivity for gamma emitters in the 100–200 keV range compared with inorganic scintillators such as sodium iodide and caesium iodide. However, the recent introduction of new technologies makes it feasible to use semiconductors such as cadmium telluride (CdTe) and cadmium zinc telluride (CdZnTe) to detect gamma rays more efficiently [6, 7, 8, 9, 10, 11, 12, 13]. They exhibit better energy resolution, better spatial resolution and very thin entry windows. This last-mentioned feature allows for detection of very low-energy beta and gamma rays. Hence, a CdTe or CdZnTe semiconductor appears to be the technology of choice for development of a prototype intraoperative imaging system [14, 15, 16, 17]. Several previous attempts at developing medical imaging devices using CdTe or CdZnTe in experimental settings have been reported [18, 19, 20, 21, 22, 23, 24]. Hand-held small gamma cameras are also under development for intraoperative lymphoscintigraphy [25, 26, 27, 28]. Two other small gamma cameras employing semiconductors were recently described: one is for CdTe [29] and one for CdZnTe [30].

We selected CdTe for our detector because to date it has not been possible to manufacture a more uniform CdZnTe crystal compared with the CdTe crystal. Furthermore, CdZnTe has poorer hole collection than CdTe. Holes tend to be trapped by impurities in the crystal structure. These disturbances of hole mobility reduce efficiency, especially in terms of energy resolution of the detector. We developed a small gamma camera using a CdTe semiconductor to enable direct imaging of suspect tissues. This could facilitate more accurate and less mutilating surgical procedures. The purpose of this study was to fabricate a small, high-resolution prototype semiconductor gamma camera (SSGC) specifically designed for use in sentinel node biopsy and related surgical applications and to perform preliminary tests on it.

Materials and methods

Design of the SSGC. We employed a CdTe semiconductor array to image gamma rays. The camera head consisted of a pixelised CdTe module attached to a collimator, the corresponding readout electronics and a housing of lead shielding (Fig. 1A). The CdTe module (Acrorad Co. Ltd., Tokyo, Japan) had 1,024 pixels with 32 rows. The CdTe crystal was grown by the traveling heater method and processed for manufacturing the semiconductor array as described previously [12, 31]. Each row consisted of 32 individual

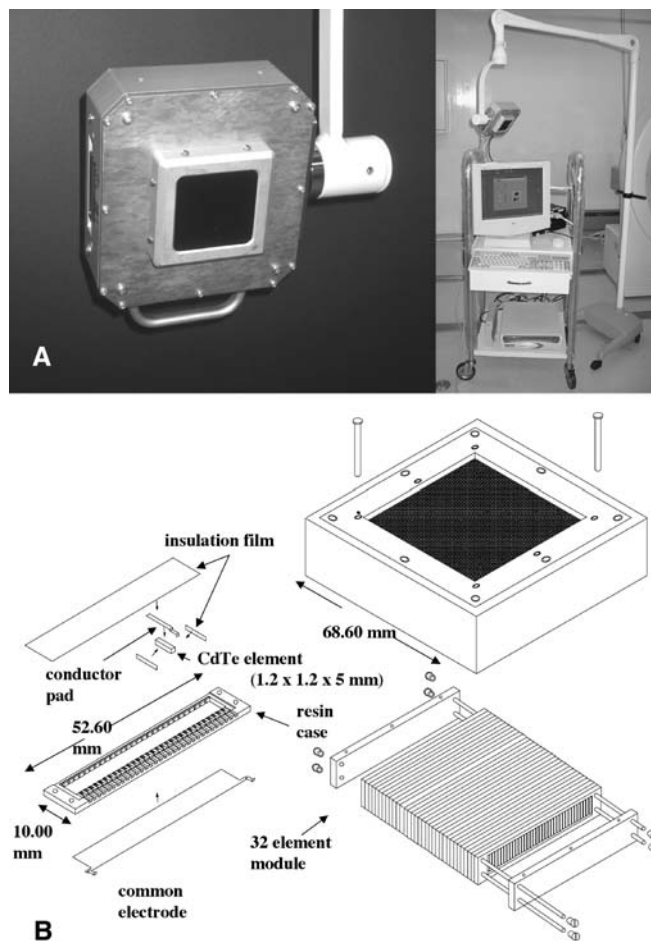


Fig. 1. A SSGC head. B Schematic of the CdTe arrays

elements that had the effective dimensions of 1.2 mm×1.2 mm and a height of 5 mm. The detector thickness was optimised for detecting 141-keV photons of technetium-99m. The rate of 141-keV energy absorption in a 5-mm thickness of CdTe is theoretically about 88%. The element fabrication was based on a Schottky CdTe detector (In/CdTe/Pt electrode system) that uses the low work function and high work function metals, indium (In) and platinum (Pt), respectively, to form ohmic contacts [10]. The spaces between neighbouring pixels and rows were 0.2 mm, and the field of view was 44.8 mm×44.8 mm. The outer dimensions of the camera head were 152 mm×166 mm×65 mm, and its weight was 2.7 kg. The collimator (Acrorad Co. Ltd., Tokyo, Japan) had a thickness of 10 mm, which comprised a stack of 100 pieces of 0.1-mm-thick tungsten mesh sheets, each having 1.2 mm×1.2 mm square openings and a space of 0.2 mm to fit the geometry of CdTe pixels. The alignment of the 100-piece tungsten mesh stack was confirmed by direct X-ray examination. For operation, a bias voltage of 500 V was applied to each element through In and Pt electrodes. The high-bias voltage afforded a decreased polarisation phenomenon [11]. As shown in Fig. 1B, an edge-on geometry was used to improve the detection of gamma rays. This geometry had a smaller distance between electrodes than that seen with a face-on geometry, which allowed application of the high-bias voltage necessary for high sensitivity and high energy resolution. The readout electronics consisted of eight pieces of application-specific integrated circuits (ASICs) [Integrated Detector and Electronics A.S. (IDE

AS), Hovik, Norway], each containing 128 channels to process analog output signal from each CdTe pixel. The energy and position signals were digitised by analog-digital converters and transferred to a personal computer (OptiPlex Gx 110, Dell Computer Corporation, Round Rock, Texas). Data acquisition was controlled by software using the LabVIEW (National Instruments, Inc., Austin, Texas) graphical programming environment.

All experiments on the SSGC were performed with collimation because the SSGC was designed as a collimated gamma camera, and the CdTe array module and collimator were assembled in a block.

Resolution. Energy resolution was measured with an 18.5-MBq ^{99m}Tc point source in air, which irradiated the entire CdTe detector from a distance of 100 cm. Energy resolution was defined as the full-width at half-maximum (FWHM) of the peak photoresponse divided by its mean amplitude.

All data were acquired by using $\pm 5\%$ energy windows about the photopeak. The spatial resolution was measured with a 1-mm inner diameter capillary tube containing ^{99m}Tc (0.37 MBq/mm; acquisition time, 600 s) placed on the surface of the collimator at distances of 2.5 cm, 5 cm and 10 cm from the surface, with or without scatter material, and with acrylic resin plates between the source and the detector surface. The plotted profiles were fitted with a Gaussian function, and the FWHM of the fitted curves was calculated as a measure of the spatial resolution.

Sensitivity. Sensitivity was established by using a 5-mm-diameter point source of ^{99m}Tc . The source was placed directly on the surface of the collimated detector.

Detector uniformity. The uniformity of the detector was determined by measuring the response to uniform ^{99m}Tc irradiation. The collimated detector was placed under an acrylic resin container (85 mm \times 85 mm \times 15 mm) filled with 444 MBq aqueous ^{99m}Tc for 600 s. The distance between the surface of the collimator and the aqueous radioactive source was 2 mm. The entire 1,024 pixels were used for characterisation of the uniformity ($\pm\sigma\%$), which was defined as the variation in the counts per pixel over the field of view.

Phantom study. A variety of phantoms were used to test the imaging characteristics of the prototype, including a point source phantom, a line source phantom, a bar phantom and a custom "S-shaped" line source phantom. The point source was 104 MBq aqueous ^{99m}Tc in a 5-ml glass vial covered with a lead shield that had a 5-mm-diameter aperture. The line sources were 200-mm-long tubes that had 1-mm (0.37 MBq/mm) and 2-mm (0.71 MBq/mm) internal diameters filled with aqueous ^{99m}Tc .

Bar phantoms (Kyoto Kagaku Co. Ltd, Kyoto, Japan) had 1.8, 2.4, 3.0 and 3.6 mm widths for spaces, and the pitches of the bars were 3.6, 4.8, 6.0 and 7.2 mm, respectively. A ^{99m}Tc source of 289 MBq was positioned 750 mm from each bar phantom, which was positioned directly on the surface of the collimated detector.

A 20-mm-tall "S" figure phantom was made from a polyethylene tube with an inside diameter of 1 mm and filled with 30 MBq of ^{99m}Tc .

Comparative scintigraphic images were acquired using an ordinary scintillation gamma camera system [SNC-5100R, matrix size 512 \times 512 pixels, field of view 51 cm \times 38 cm, NaI(Tl) crystal, energy resolution 10.4% (^{99m}Tc), spatial resolution 3.5 mm (^{99m}Tc) (Shimadzu, Kyoto, Japan)]. Phantoms were placed directly on the surface of the gamma camera, which was equipped with a parallel-hole low-energy (high-resolution) collimator.

In all phantom studies, the SSGC was equipped with the same collimator as described in the design section.

Phantom simulation study. We also used phantoms to simulate sentinel lymph nodes. When a typical sentinel lymph node biopsy is performed for breast cancer under clinical conditions, only a very small amount of radiopharmaceutical accumulates in the sentinel lymph node(s). Phantoms simulating cancerous breast tissues under these conditions were constructed from acrylic resin-containing spherically shaped holes with internal diameters of 5, 10 and 15 mm. For sentinel node simulation, two spheres (diameters: 5 mm, 10 mm) were filled with 0.15 MBq of ^{99m}Tc each and placed at 0, 10, 30 and 50 mm below the water surface. The tested node-to-node separations were 15, 20, 30 and 45 mm. All radioactivity was counted for 15 s. The same spheres were imaged 18 h and 24 h later, again using a 15-s integration time.

We tested the so-called shine-through effect by conducting a simulation to determine the minimum separation between node and injection site that could be resolved by the SSGC. The shine-through effect is the phenomenon in which a large volume of radioactivity in the injection site interferes with counting of the smaller radioactivity of sentinel nodes in close proximity to the injection site. Two spheres measuring 5 mm and 15 mm in diameter represented the sentinel node (0.15 MBq) and injection site (100 MBq), respectively. A simulated sentinel lymph node was positioned at the following depths under water: 0, 10, 30 and 50 mm. A sphere representing the injection site was placed at 10 mm under water. The distance between the centres of the injection site and the sentinel lymph node were adjusted over the following ranges: 15, 20, 30 and 45 mm.

Two researchers who were blinded to the locations of simulated nodes interpreted images independently with respect to visibility of nodes. When the two observers agreed that the node was visible, the node was evaluated as resolved. Regions of interest (ROIs) over the simulated nodes and background, of the same size as the node region, were established to quantify the uptake. Radioactivity in each ROI was counted for 15 s. The radioactivity was expressed as the ratio of the node to the background counts (node/BG ratio). The count profiles of images were drawn through the nodes and injection sites in a test of the shine-through effect.

Patient study. ^{99m}Tc -phytate [32] was injected 24 h before surgery in a 71-year-old woman who had known intraductal papillary carcinoma of the right breast. Radionuclide studies are preferentially performed using small colloids, which have limited availability in Japan. Four 37-MBq injections were made intradermally above, below and on each side of the primary site. The patient underwent total mastectomy and axillary lymphatic dissection. The excised en bloc breast and axillary lymph tissue was imaged immediately after surgery with the SSGC and conventional scintillation gamma camera for comparison.

In another clinical example, dynamic blood flow images were taken in a patient with oral cancer who was studied by bone scintigraphy. The SSGC was placed on the forearm of the patient to obtain serial images of the injection site every 0.5 s immediately after intravenous injection of ^{99m}Tc -methylene diphosphonate.

Six other patients were also studied. They had the following conditions: oral squamous cell carcinoma (two cases), thyroid adenoma (one case), osteomyelitis of the mandible (one case), sialadenitis of the parotid gland (one case) and temporomandibular joint dysfunction (one case). Clinical images were produced 4 h after intravenous administration of ^{99m}Tc -MDP or ^{99m}Tc -pertechnetate using the SSGC and conventional scintillation camera to provide

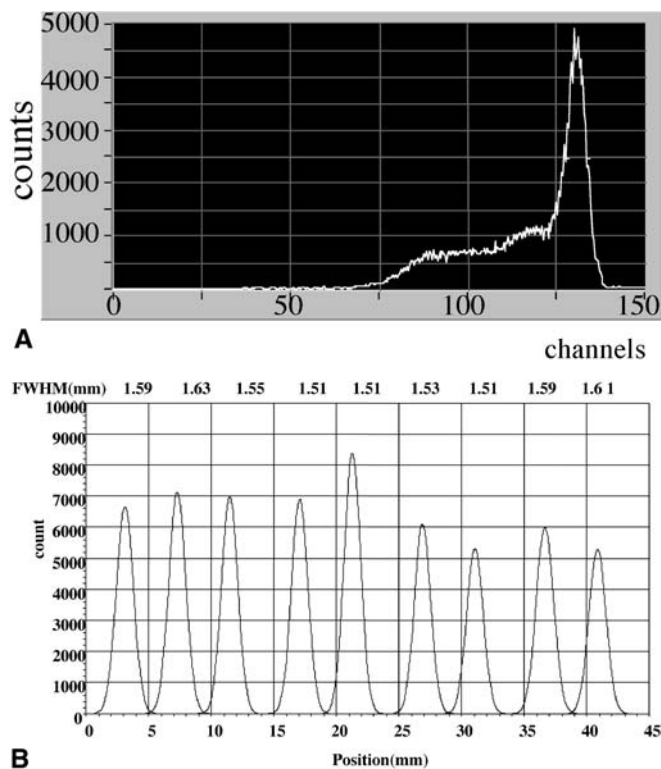


Fig. 2. **A** The mean energy resolution of the SSGC was 7.8% (^{99m}Tc , 140 keV). The energy resolution was computed from the FWHM and the energy of the photon E . The resolution of a single element situated in the centre of the detector was 4.2%. **B** The spatial resolution was measured with a line source of ^{99m}Tc , and plotted profiles were fitted with a Gaussian function. The FWHMs of the fitted curves are shown, with an average FWHM of 1.56 mm

test and control data, respectively. Written informed consent was obtained from all eight patients after the nature and possible risks of their voluntary participation had been explained. The ethics committee of the Nippon Dental University School of Dentistry at Niigata approved all research involving the patients.

Results

Resolution

The energy spectrum obtained with ^{99m}Tc (140 keV) is shown in Fig. 2A. The measured energy resolution (FWHM) for a single element at the centre of the field of view was 4.2%, and the energy resolution of the CdTe detector was 7.8%. The results documented variation in energy resolution among elements. Insufficient energy calibration in this prototype setting accounts for the variation between individual elements of the device. The spatial resolution, represented by FWHM, had a mean value of 1.56 ± 0.05 mm when the capillary tube was placed on the surface of the detector. Image profiles of line sources are shown in Fig. 2B. The FWHM was

3.89 ± 0.09 mm, 6.31 ± 0.25 mm and 11.21 ± 0.42 mm without scatter material and 4.06 ± 0.27 mm, 7.24 ± 0.58 mm and 12.63 ± 0.39 mm with scatter material at distances of 2.5 cm, 5 cm and 10 cm, respectively.

Sensitivity

The detection efficiency of the SSGC was 0.30 counts/s per kBq (^{99m}Tc). For purposes of comparison, we used the scintillation camera with a parallel-hole low-energy (high-resolution) collimator in all phantom and clinical imaging studies. The detection efficiency of this scintillation camera was 0.08 counts/s per kBq (^{99m}Tc) on the same geometry as for SSGC.

Detector uniformity

The average count per pixel of the entire 1,024 pixels in the detector was $30,195 \pm 1,348$. The uniformity ($\pm \sigma\%$) was 4.5%.

Point source

The 5-mm diameter point source of ^{99m}Tc , with an activity of 104 MBq/ml, was placed directly on the prototype detector surface. Images produced by the point source were easily resolved from the background with acquisition times of as short as 2 s.

Line source

The 200-mm-long line sources, with 2 mm and 1 mm diameters, also were easily resolved by the SSGC after a 2-s acquisition time.

Bar phantom

Resolution estimates were produced from images of four types of bar phantom. Images produced by the SSGC integrated over an exposure time of 2 s allowed visual resolution of the bars produced with the most challenging phantom (slit dimension 1.8 mm, pitch 3.6 mm). The conventional scintillation camera could not resolve the bars of the phantom irrespective of the amount of time used for integration (Fig. 3A).

Moire effects were not apparent in bar phantom studies with different bar angle projections.

“S” figure phantom

We compared test and control images of the “S” figure phantom, which was placed directly on the surface of

Fig. 3. A Images of the bar phantoms (*upper left to lower left, clockwise*): slit dimension 3.6 mm, pitch 7.2 mm; slit dimension 3.0 mm, pitch 6.0 mm; slit dimension 2.4 mm, pitch 4.8 mm; and slit dimension 1.8 mm, pitch 3.6 mm. The conventional scintillation camera could not resolve the bars of the phantom, especially at the slit dimension 1.8 mm, pitch 3.6 mm, irrespective of the amount of time used for integration. **B** Images obtained from a 20-mm-tall “S” figure phantom made from a 1-mm-diameter polyethylene tube and filled with 30 MBq ^{99m}Tc , that was placed directly on the surface of each camera with a 2-s acquisition time. The image obtained by SSGC (*left*) is much clearer than that obtained with a conventional scintillation camera (*right*)

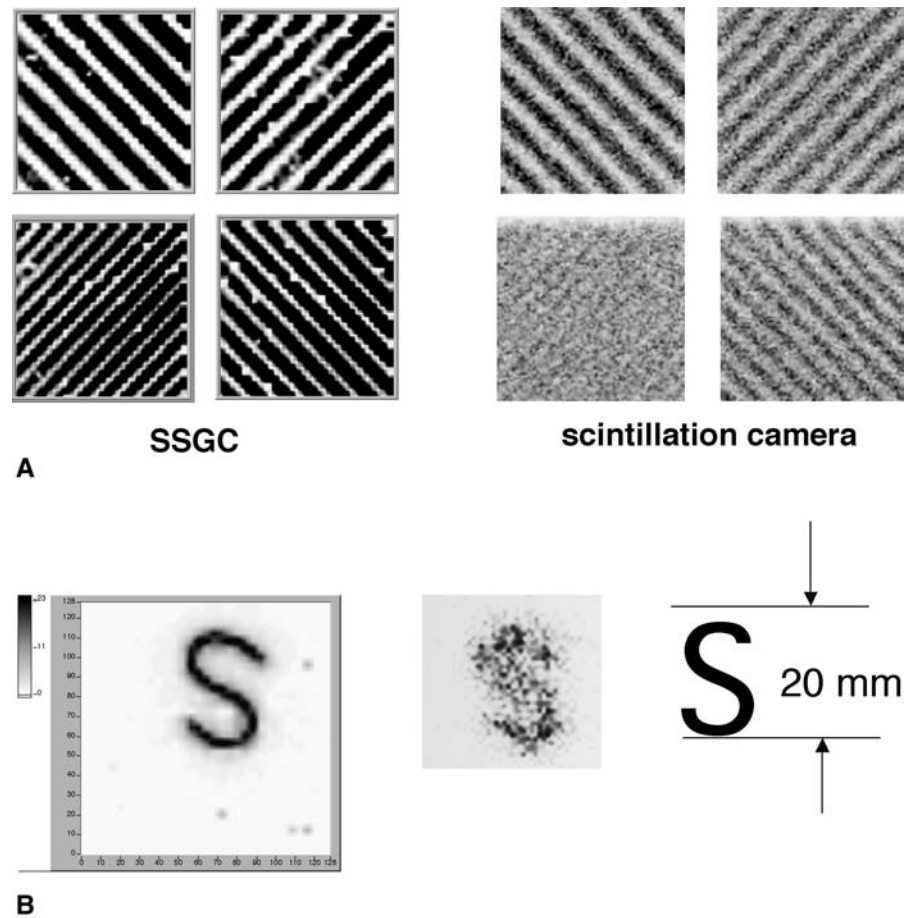


Table 1. Node to background ratios (node/BG ratios) of the simulated sentinel nodes

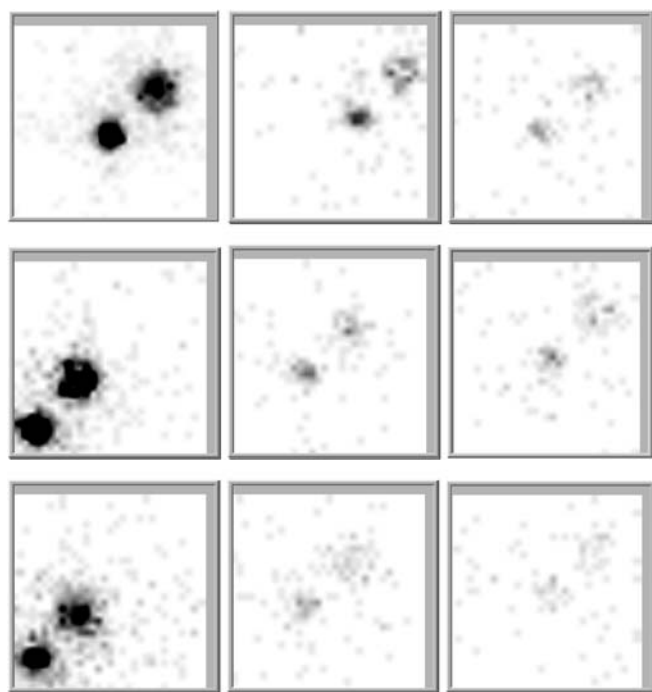
Depth	0 h		18 h		24 h	
	ϕ 5 mm	ϕ 2.5 mm	ϕ 5 mm	ϕ 2.5 mm	ϕ 5 mm	ϕ 2.5 mm
0 mm	32.2	48.5	11.8	12.2	10.9	11.2
10 mm	27.2	48.0	11.8	12.3	10.0	10.7
30 mm	26.6	32.9	11.0	11.7	8.3	8.5

each camera under the same conditions. After 2 s of integration time, the image obtained by the SSGC resolved much more easily than that produced by the conventional scintillation camera, which was serving as the control (Fig. 3B).

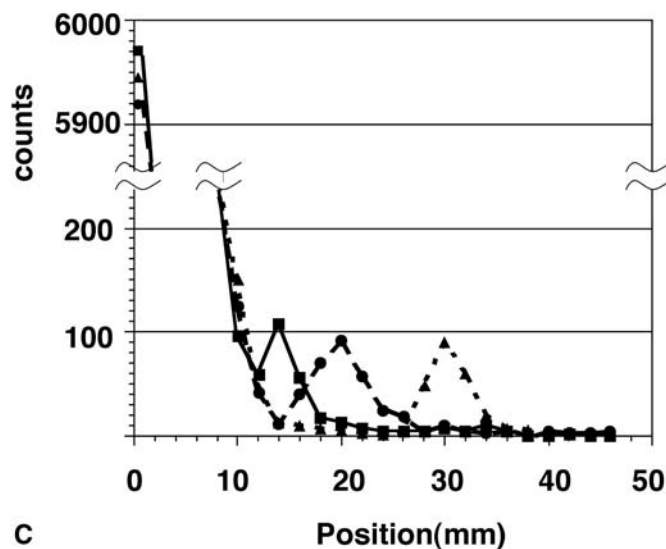
Simulation study

The SSGC reliably detected the simulated nodes at up to a 30-mm water depth over 18 h of decay. Even after 24 h, two of the simulated sentinel nodes were recognisable in a water depth of up to 10 mm after employing the same integration time of 15 s (Fig. 4A). Node/BG ratios of all visually recognised nodes were greater than 10 (Table 1).

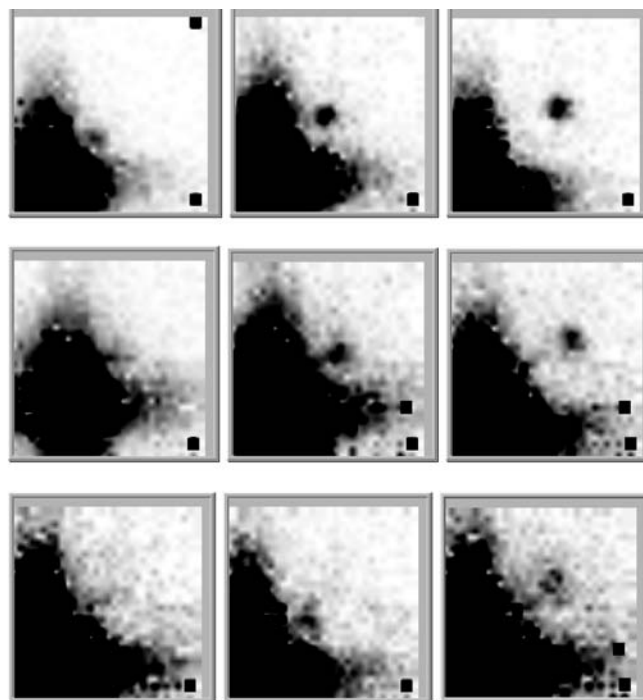
The two sources of radioactivity in the shine-through effect simulation could not be reliably distinguished when their horizontal centre-to-centre distance was 15 mm, irrespective of water depth, at an integration time limited to 15 s. However, when the distance was increased horizontally to 20 mm, the two sources resolved using SSGC (Fig. 4B). Count profiles are shown in Fig. 4C. Ratios of the peak count of the simulated node to the bottom count, which was the lowest count between the injected site and the node (shine-through count), were 11.4 and 30.0 at 20-mm and 30-mm separation, respectively. The ratio at 15-mm separation was 1.8, with difficulties in resolving activities spatially. Activities could be resolved spatially after 24 h when the foci were 30 mm and 45 mm apart at water depths of 10 and 30 mm using the same 15-s integration time, but not at



A



C



B

Fig. 4. **A** Images of the sentinel node-to-sentinel node separation, with 15 mm between the centres of the nodes (simulated). Each ^{99m}Tc image was acquired for 15 s. The *top row* of images was taken at 0 mm underwater depth from the surface of the collimator immediately after preparation of 0.15 MBq of ^{99m}Tc (*left*), at 18 h after preparation (*middle*) and at 24 h after preparation (*right*). The *middle row* shows results at an underwater depth of 10 mm, and the *bottom row*, results at an underwater depth of 30 mm, over the same time course as in the *top row*. **B** Images of a pair of lesions simulating a 100-MBq injection site (INJ) and a 0.15-MBq sentinel lymph node (SN). Each image was acquired for 15 s. The INJ-to-SN separation is 15 mm (*left column*), 20 mm (*middle column*) and 30 mm (*right column*). Images are from underwater depths of 0 mm (*top row*), 10 mm (*middle row*) and 30 mm (*bottom row*). A 15-mm-diameter sphere simulating the INJ was placed at a depth of 10 mm underwater. **C** The corresponding profiles of the shine-through test images. The profiles were drawn through the line over the SN and INJ with 15-mm, 20-mm and 30-mm separations and 0-mm depth images shown in **B**

closer separations or deeper source depths with shine-through counts lower than 10.

The spherical source simulating the injection site was visualised on images not as circular, but rather as diamond shaped. Because of the difference in thickness of accumulated collimator septa, photon penetration changed at different projections (Fig. 4B).

A few of dead or black-out pixels that appeared in the images (Fig. 4B) were due to the prototype setting in which some pixels did not adequately contact ASICs. Similar black-out pixels appeared in other images (Fig. 7A).

Patient studies

When the SSGC was placed on the surface of the excised bloc specimen of the right breast and axillary lymphatic tissue excised from the breast cancer patient, a secondary radioactive focus (later confirmed to be a sentinel node) located in the axillary region was resolved. Figure 5 shows the performance differences between the SSGC and the conventional scintillation camera, used as a control, under similar conditions. Using comparable or even shorter integration times and 180 s of imaging, the activity of ^{99m}Tc -phytate accumulated in the newly discovered sentinel node was depicted more clearly by the

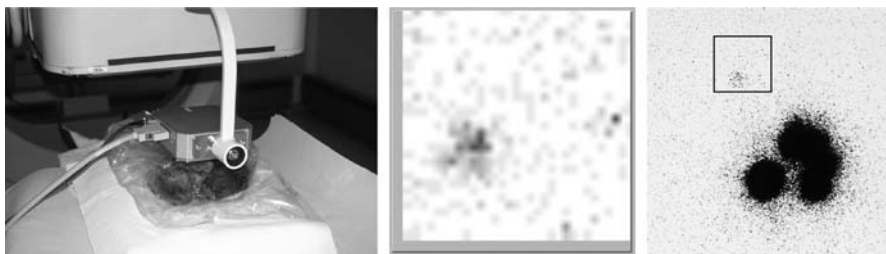


Fig. 5. Patient study for sentinel lymph node biopsy. Excised tissue of the right breast and axillary tissue of a 71-year-old woman with breast cancer was placed under the SSGC (*left*). Unlike in the image obtained using a conventional scintillation camera with 600 s integration (*right*), the radioactivity of the sentinel node is clearly shown by SSGC with a 180-s acquisition time, even at 30 h after injection of 100 MBq of ^{99m}Tc -phytate in the primary lesion (*middle*)

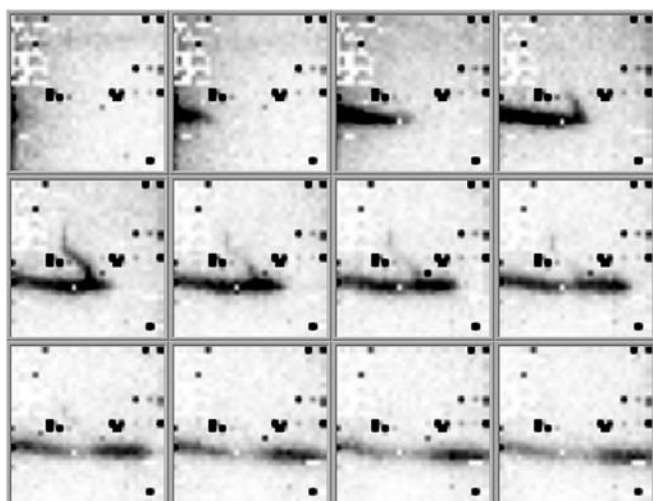


Fig. 6. Dynamic images of blood flow in the forearm of a patient who underwent bone scintigraphy. The serial images clearly display the blood flow of ^{99m}Tc -MDP in the median cephalic vein. Note the small ramification vessel from the vein

SSGC than by the scintillation camera, even 30 h after injection.

Another clinical example demonstrated even more subtle changes. Images of the injection site were obtained every 0.5 s by positioning the SSGC on the forearm of a patient who underwent bone scintigraphy. Serial analysis of the resulting images clearly indicated the dynamics of blood flow of ^{99m}Tc -MDP in the median cephalic vein (Fig. 6). We found several black-out pixels in the bloodstream images only when a large amount of radionuclide was imaged. This may have been due to a large amount of radionuclide affecting proper functioning of the ASICs.

In another patient, ^{99m}Tc -pertechnetate images showed a cold region in the left lobe caused by a thyroid adenoma, as well as thyroid accumulation of the tracer. SSGC images were taken for 2, 15, 30 and 60 s. The 15-, 30-

and 60-s SSGC images revealed more details than the conventional scintillation camera images (Fig. 7). The SSGC clearly showed the right parotid gland in sialoscintigraphy, clearly demarcated the mandible and documented the difference in intensity in the region of osteomyelitis that was shown with bone scintigraphy. The accumulation of ^{99m}Tc -MDP in the right temporomandibular joint was revealed much more clearly by SSGC than by the conventional scintillation camera.

Discussion

To date, CdTe and CdZnTe are the detectors of choice, despite some drawbacks. The polarisation phenomenon with CdTe is the major cause of energy resolution degradation and reduced peak efficiency [33]. Fortunately, this phenomenon can be resolved by operating at either low temperature or high-bias voltage or, most practically, by temporarily shutting down the bias voltage [10]. CdZnTe has low mobility/lifetime of holes compared with electrons [34]. The hole trapping can be a serious disadvantage for signal collection. Large-scale production has been achieved, but quality control for maintenance of highly uniform CdZnTe production remains difficult. This impurity renders a large amount of hole trapping in cracks or contaminated ingredients. However, new technologies have excellent potential as substitutes for ordinary scintillation detectors in clinical imaging.

The introduction of the Schottky electrodes made of In allows our SSGC to be supplied with high voltage and decreases leaking current. Furthermore, advances in crystal growth technology, array technology with miniaturising pixels, multichannel front-end electronics and data acquisition systems have made it possible for our SSGC to achieve high energy and spatial resolution.

When a typical sentinel lymph node biopsy is performed under clinical conditions, only a very small amount of radiopharmaceutical accumulates in the sentinel node(s) of the patient who has a malignancy. Although the injection methods and ^{99m}Tc -labelled particles differed, the average percentages of injected dose per lymph node in various studies were 0.36%, 0.9% and 0.60% in patients with malignant melanoma, breast carcinoma and breast carcinoma, respectively [35, 36, 37]. In a study of 60 melanoma patients, uptake in the sentinel node ranged from 0.0013% to 6.8% of the injected tracer dose [35]. In breast cancer, the range was 0.001%

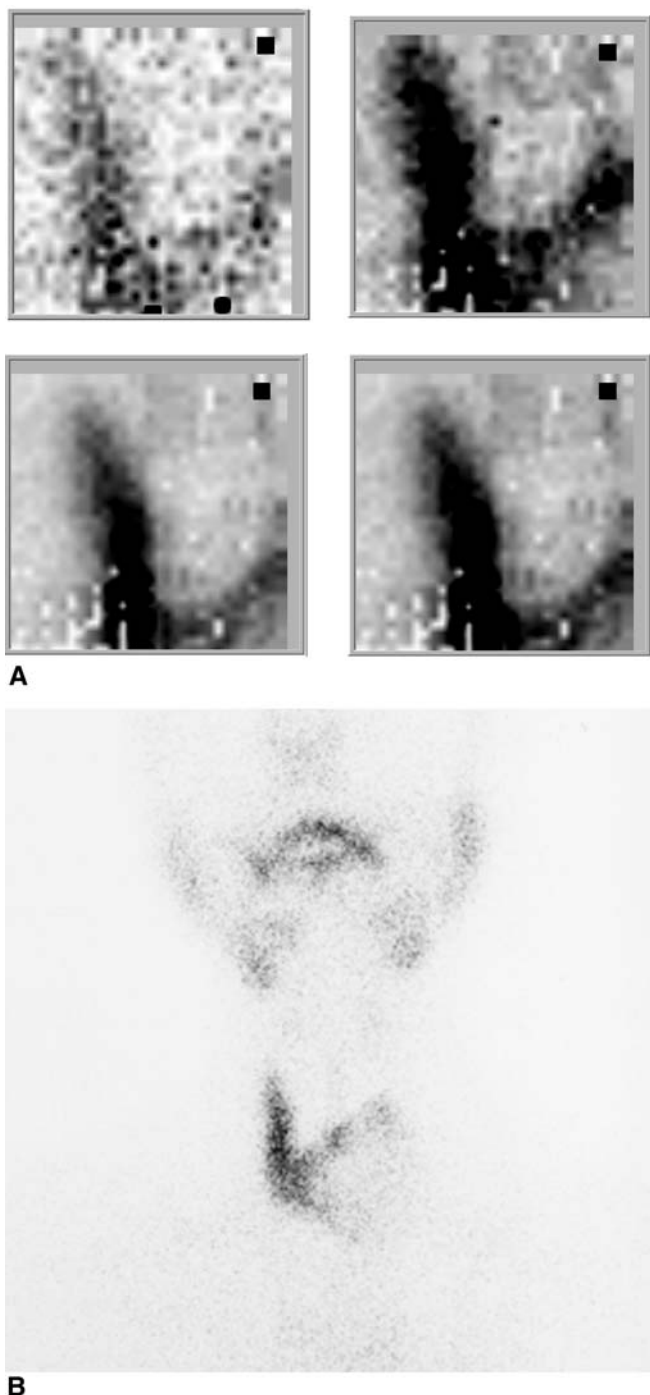


Fig. 7A, B. Imaging of a thyroid adenoma. **A** ^{99m}Tc -pertechnetate images show a cold region in the left lobe, caused by the tumour, and thyroid accumulation of the tracer, with images taken for 2, 15, 30 and 60 s (*upper left, upper right, lower left and lower right, respectively*) acquisition times. **B** An image taken with the conventional scintillation camera

to 2.5% [37, 38]. Some surgeons estimate the percentage of injected dose per lymph node to be about 0.15%. Hence, it is important to determine the reliability of the SSGC in detecting such small concentrations of radioactivity under simulated clinical conditions. The SSGC re-

liably detected small amounts of activity of the simulated nodes (0.15% of the injected 100-MBq dose) at up to a 30-mm underwater depth after 18 h. Even after 24 h, when the radioactivity had decreased to 1/16th of its initial value (0.0094 MBq), two of the simulated sentinel nodes could still be recognised (Fig. 4A).

Too much radioactivity from the injection site interferes with detection of a small amount of nodal radioactivity situated close to the injection site when exploring sentinel lymph nodes with the gamma probe. We tested this phenomenon, which is referred to as “shine-through,” by conducting a simulation to determine the minimum separation between node and injection site that could be resolved by the SSGC. The two sources of radioactivity could not be reliably distinguished when their centre-to-centre distance was 15 mm or less, irrespective of water depth, at an integration time of 15 s. However, when the separation distance was increased to 20 mm, the two sources could be resolved (Fig. 4B). After 24 h, we could spatially resolve focal activities that were 30 mm and 45 mm apart at a water depth of 10 and 30 mm using the same 15-s integration time. In this situation, the activity of the simulated node was 0.0094 MBq and that of the injection site was 6.25 MBq of ^{99m}Tc . In another simulation study for gamma probes, the minimum node-to-injection site separation for all tested probes was more than 78 mm, with the activity of a 30-mm deep node being 0.0125 MBq and that of a 5-mm deep injection site being 2.5 MBq [39]. It is of interest that in typical clinical applications, a gamma probe is relatively limited in its ability to isolate adjacent signals. This fundamental limitation stems from the fact that a blind probe cannot be designed with sufficient collimation to assure spatial resolution comparable to the SSGC without unduly restricting its capacity to sample clinically practical tissue volumes. Accordingly, radioactivity near the injection site tends to mask accumulations of radionuclide tracer into sentinel nodes and related tissues when they lie in close proximity.

The SSGC was able to resolve a sentinel node of a patient who had breast cancer 30 h after injection of ^{99m}Tc -phytate (Fig. 5). The image taken by the SSGC was much clearer than that obtained by a conventional scintillation gamma camera at a shorter integration time. These results confirm the potential for this new SSGC in sentinel lymph node biopsy. However, we believe that the conventional scintillation camera is still necessary for localisation of sentinel node(s) during preoperative lymphoscintigraphic study on a large field of the breast or other regions, with the SSGC introduced into the sentinel lymph node biopsy.

In a dynamic study of blood flow in the forearm, serial images integrated at 0.5 s clearly documented the flow of ^{99m}Tc -MDP in a small ramification of the median cephalic vein (Fig. 6). This capability demonstrates the potential of the SSGC to resolve diagnostically relevant information using relatively short image acquisition times,

which may make possible a variety of interactive applications requiring near real-time imaging capabilities.

^{99m}Tc -pertechnetate images obtained by SSGC showed a cold region in the left lobe caused by a thyroid adenoma, as well as thyroid accumulation of the tracer. SSGC images revealed more detail than the conventional scintillation camera image (Fig. 7). The SSGC also clearly showed the parotid gland, mandible and temporomandibular joint more clearly than did the conventional scintillation camera. The size of the detector allows it to be positioned close to small body parts or complex anatomical regions. Accordingly, the SSGC holds potential for application in the diagnosis of cervical, oral and maxillofacial diseases. Researchers have applied small CdTe probes in experimental dental, bone healing and temporomandibular joint studies in dogs and in human periodontal studies [40, 41, 42, 43]. The quality of high-resolution images obtained with the SSGC offers promise for animal and clinical nuclear medicine studies in the oral and maxillofacial region.

We encountered some minor imaging problems with the detector. A small number of dead pixels and black-out pixels in some images were due to the prototype setting in which some pixels did not adequately contact ASICs. Because of rejected signals from pixels containing high leakage current, some pixels did not properly show the radioactivity. The black-out pixels also appeared on the bloodstream dynamic study (Fig. 6). This was due to a large amount of radionuclide interfering with proper functioning of the ASICs. Furthermore, variation occurred in energy resolution among elements due to insufficient calibration. These problems will be addressed by improved technique in the future version of the SSGC designed for clinical use. The new SSGC head will have a conformation that aids in manoeuvrability at surgery. The size of the SSGC detector dimension that faces the target tissue or operative field will be reduced by architectural design for the configuration of the detector and connecting ASICs.

In conclusion, we have developed a prototype, relatively small, high-resolution, semiconductor gamma camera intended for possible use in radioguided surgery. The SSGC resolved small amounts of radioactivity consistent with activities acquired by breast sentinel nodes using relatively short acquisition times. Simulated sentinel nodes could be isolated from radioactivity at levels consistent with accumulations typically measured at a clinical injection site, even when nodes were situated a short distance from the confounding source of radioactivity, thus minimising the "shine-through" effect. The SSGC may offer advantages over current techniques for isolating sentinel lymph nodes for biopsy. It also might aid surgeons in identifying target tissues when performing radioguided surgery. A further potential application for this camera is in diagnosis, particularly of small, superficial lesions situated in tissues or organs such as the thyroid gland, parathyroid gland, jaws, facial bones, salivary glands and joints.

Acknowledgements. We gratefully acknowledge the cooperation of Eiko Sakata, MD, Masahiro Ohtake, MD, PhD, and Keisuke Yoshida, MD, PhD, in studying the sentinel lymph node biopsy of a patient with breast carcinoma. The authors also thank Richard L. Webber, DDS, PhD, for his helpful comments.

This study was supported in part by a Grant-in-aid for Scientific Research from the Ministry of Education, Science, Sports and Culture of Japan (B2-11557142).

References

- Burak WE Jr, Boso M, Thurston MO, Martin EW Jr. Surgical application of gamma-detecting probes. *Surg Tech Int* 1996; 5:259–264.
- Morton DL, Wen D-R, Wong JH, et al. Technical details of intraoperative lymphatic mapping for early stage melanoma. *Arch Surg* 1992; 127:392–399.
- Krag DN, Meijer SJ, Weaver DL, et al. Minimal-access surgery for staging of malignant melanoma. *Arch Surg* 1995; 130:654–658.
- Krag D, Weaver D, Ashikaga T, et al. The sentinel node in breast cancer: a multicenter validation study. *N Engl J Med* 1998; 339:941–946.
- Veronesi U, Paganelli G, Viale G, et al. Sentinel lymph node biopsy and axillary dissection in breast cancer: results in a large series. *J Natl Cancer Inst* 1999; 91:368–373.
- Matherson KJ, Barber HB, Barrett HH, et al. Progress in the development of large-area modular 64×64 CdZnTe imaging arrays for nuclear medicine. *IEEE Trans Nucl Sci* 1988; 45:354–358.
- Siffert P. Cadmium telluride and related materials as X- and gamma-ray detectors: a review of recent progress. *Proc Soc Photo-Opt Instrum Engin* 1994; 2305:98–109.
- Barber HB, Marks DG, Apotovsky BA, et al. Progress in developing focal-plane-multiplexer readout for large CdZnTe arrays for nuclear medicine applications. *Nucl Instrum Methods Phys Res* 1996; A380:262–265.
- Butler JF. Novel electrode design for single-carrier charge collection in semiconductor nuclear radiation detectors. *Nucl Instrum Methods Phys Res* 1997; A396:427–430.
- Matsumoto C, Takahashi T, Takizawa K, Ohno R, Ozaki T, Mori K. Performance of a new Schottky CdTe detector for hard X-ray spectroscopy. *IEEE Trans Nucl Sci* 1998; 45:428–432.
- Takahashi T, Hirose K, Matsumoto C, Takizawa K, Ohno R, Ozaki T, Mori K, Tomita Y. Performance of a new Schottky CdTe detector for hard x-ray spectroscopy. *Proc Soc Photo-Opt Instrum Engin* 1998; 3446:29–37.
- Funaki M, Ozaki T, Satoh K, Ohno R. Growth and characterization of CdTe single crystals for radiation detectors. *Nucl Instrum Methods* 1999; A436:120–126.
- Scheiber C. CdTe and CdZnTe gamma ray detectors in nuclear medicine *Nucl Instrum Methods* 2000; A448:513–524.
- Dusi W, Caroli E, Stephen JB, Chirco P. CdTe room temperature semiconductor detectors and their suitability for medical applications. *Phys Med* 1993; 9:195–200.
- Hoffman EJ, Tornai MP, Janacek M, Patt BE, Iwanczyk JS. Intraoperative probes and imaging probes. *Eur J Nucl Med* 1999; 26:913–935.
- Nakamura N. Technical trend of semiconductor detector for nuclear medicine [in Japanese]. *Med Imag Technol* 2000; 18:3–8.
- Yamakawa T. New trend of semiconductor detector [in Japanese]. *Kaku Igaku* 1997; 34:569.

18. Entine G, Luthmann R, Mauderli W, Fitzgerald LT, Williams CM. Cadmium telluride gamma camera. *IEEE Trans Nucl Sci* 1979; NS-26:552–558.
19. Allison JD. Cadmium telluride matrix gamma camera. *Med Phys* 1980; 7:202–206.
20. Woolfenden JM, Barber HB. Radiation detector probes for tumor localization using tumor-seeking radioactive tracers. *Am J Roentgenol* 1989; 153:35–39.
21. Scheiber C. New developments in clinical applications of CdTe and CdZnTe detectors. *Nucl Instrum Methods Phys Res* 1996; A380:385–391.
22. Marks DG, Barber HB, Barrett HH, Eskin JD. Maximum-likelihood estimation for a 64×64 CdZnTe array [abstract]. *J Nucl Med* 1998; 39(Suppl):173P.
23. Takayama T, Nakamura N, Motomura N, Mori, I, Ozaki T, Ohno R. Feasibility study of CdTe semiconductor detector for gamma camera: evaluation of planar images [in Japanese]. *Kaku Igaku* 2000; 37:181–187.
24. Mori I, Takayama T, Motomura N. The CdTe detector and its imaging performance. *Ann Nucl Med* 2001; 15:487–494.
25. Patt BE, Tornai MP, Iwanczyk JS, Levin CS, Hoffman EJ. Development of an intraoperative gamma camera based on a 256-pixel mercuric iodine detector array. *IEEE Trans Nucl Sci* 1997; 44:1242–1248.
26. Menard L, Charon Y, Solal M, et al. A compact high resolution gamma camera for intra-operative surgical use. *IEEE Trans Nucl Sci* 1998; 45:1293–1297.
27. Pitre S, Menard L, Charon Y, et al. A high resolution hand-held gamma camera for cancer surgery [abstract]. *J Nucl Med* 2001; 42(Suppl):202P.
28. MacDonald LR, Patt BE, Iwanczyk JS, et al. High-resolution hand-held gamma camera. *Proceedings of the international symposium on optical science and technology, the Society of Photo-Optical Instrumentation Engineers' 45th annual meeting*. 2000; 4508:1–12.
29. Baumann E, Bruin NM, Ijbema T, Fougères P, Teule GJ. A prototype: pixelized small imaging CdTe probe for intra-operative use [abstract]. *J Nucl Med* 2001; 42(Suppl):203P.
30. Parnham KB, Grosholz J, Davies RK, Vydrin S, Cupec CA. Development of a CdZnTe-based small field-of-view gamma camera. *Proceedings of the international symposium on optical science and technology, the Society of Photo-Optical Instrumentation Engineers 46th annual meeting*. 2001; 4508:173.
31. Ozaki T, Iwase Y, Takamura H, Ohmori M. Thermal treatment of CdTe surfaces for radiation detectors. *Nucl Instrum Methods* 1996; A380:141–144.
32. Alavi A, Staum MM, Shesol BF, Bloch PH. Technetium-99m stannous phytate as an imaging agent for lymph nodes. *J Nucl Med* 1978; 19:422–426.
33. Bell RO, Entine G, Serreze HB. Time dependent polarization of CdTe gamma-ray detectors. *Nucl Instrum Method* 1974; 117:267–271.
34. Schlesinger TE, James RB. Semiconductors for room temperature nuclear detector applications. In: Willardson RK, Weber ER, Schlesinger TE, Jones RB, eds. *Semiconductors and semi-metals 43*. San Diego, Calif: Academic Press, 1995.
35. Kapteijn BA, Nieweg OE, Muller SH, et al. The validation of gamma probe detection of the sentinel node in melanoma. *J Nucl Med* 1997; 38:362–366.
36. De Ciccio C, Cremonesi M, Luini A, et al. Lymphoscintigraphy and radio-guided biopsy of the sentinel axillary node in breast cancer. *J Nucl Med* 1998; 39:2080–2084.
37. Rink T, Heuser T, Fitz H, Schroth H-J, Weller E, Zippel HH. Lymphoscintigraphic sentinel node imaging and gamma probe detection in breast cancer with Tc-99m nanocolloidal albumin: results of an optimized protocol. *Clin Nucl Med* 2001; 26: 293–298.
38. Nieweg OE, Tanis PJ, de Vries JDH, Valdes Olmos RA, Kroon BBR, Hoefnagel CA. The sentinel node in melanoma: present controversies. *The 48th Society of Nuclear Medicine Annual Meeting, 2001 Handout Book*. 2001:94–103.
39. Britten AJ. A method to evaluate intra-operative gamma probes for sentinel lymph node localization. *Eur J Nucl Med* 1999; 26:76–83.
40. Jeffcoat MK, Williams RC, Kaplan ML, Goldhaber P. Tetracycline treatment of periodontal disease in the beagle dog: correlation between bone-seeking radiopharmaceutical uptake and rate of bone loss. *J Periodontal Res* 1982; 17:545–551.
41. Jeffcoat MK, Williams RC, Holman BL, English R, Goldhaber P. Detection of alveolar bone destruction in human periodontal disease by analysis of radio-pharmaceutical uptake after a single injection of 99m-Tc-methylene diphosphonate. *J Periodontal Res* 1986; 21:677–684.
42. Tsuchimochi M, Hosain F, Engelke W, Zeichner SJ, Ruttimann UE, Webber RL. Studies on focal alveolar bone healing with technetium (Tc)-99m labeled methylene diphosphonate and gold-collimated cadmium telluride probe. *Oral Surg Oral Med Oral Pathol* 1991; 71:110–115.
43. Engelke W, Tsuchimochi M, Ruttimann UE, Hosain F. Assessment of bone remodeling in the temporomandibular joint by serial uptake measurement of technetium 99m-labeled methylene diphosphonate with a cadmium telluride probe. *Oral Surg Oral Med Oral Pathol* 1991; 71:357–363.